



Cite this: *Green Chem.*, 2025, **27**, 13089

## A dynamic sulfur-rich network from silicone industry waste

Zixiao Wang, †<sup>a</sup> Yuanyuan Qiu, †<sup>a</sup> Zheju Cheng, <sup>a</sup> Honglu Huang, <sup>a</sup> Yang Sui, <sup>b</sup> Xin Liu, <sup>a</sup> Yijie Yang, <sup>a,c</sup> Yue Lu, <sup>a</sup> Huie Zhu, <sup>c</sup> Qingqing Ji \*<sup>a</sup> and Jiajun Yan \*<sup>a</sup>

Industrial waste accumulation poses significant environmental challenges. Dimethyldivinylsilane, a notable side product of the silicone industry, is left without a specific use. Meanwhile, sulfur, the most common byproduct of the petrochemical industry, is frequently in surplus despite being largely utilized for sulfuric acid production. This study employed the inverse vulcanization technique to upcycle these two waste streams into sulfur-rich dynamic polymer networks. The silicon-based crosslinker contributed to distinct dynamic behaviors for the synthesized polymers compared to other inverse vulcanized networks, resulting in a variety of accessible morphologies depending on specific processes. The produced sulfur-rich malleable film was found to enhance the high-temperature performance of monolayer MoS<sub>2</sub> transistors by healing the sulfur vacancies and suppressing the switching hysteresis. This investigation highlights the potential for industrial waste upcycling and its application in the future design of materials and devices.

Received 6th June 2025,  
 Accepted 15th September 2025  
 DOI: 10.1039/d5gc02864g  
[rsc.li/greenchem](http://rsc.li/greenchem)

### Green foundation

1. Our work transforms two major industrial waste streams (dimethyldivinylsilane and sulfur) into a high-value functional material using solvent-free inverse vulcanization.
2. We achieved atom-efficient conversion of low-value waste into a dynamic polymer. Applied as a coating, it extends the lifespan of monolayer MoS<sub>2</sub> transistors as a candidate for next generation electronics by healing defects.
3. Further research will focus on low-energy, scalable synthesis, exploring diverse applications, and enabling closed-loop material recycling after end-of-life.

## Introduction

Recently, the emphasis on sustainable development has heightened the need for efficient recycling of industrial byproducts. In this context, two industrial wastes, dimethyldivinylsilane (DMDVS) and sulfur, are considered here. DMDVS is an inevitable side-product in the production of 1,1,3,3-tetramethyl-1,3-divinyldisiloxane (DVDSi) through the Wurtz–Fittig process (Fig. 1a).<sup>1–4</sup> Silicon, the second most abundant element in the Earth's upper continental crust,<sup>5</sup> underpins a well-developed silicon industry, in which DVDSi serves as a critical raw material; notably, it also serves as the ligand in Karstedt's catalyst for hydrosilylation, one of the largest-scale applications of homogeneous catalysis.<sup>6,7</sup> The global DVDSi production is consistently growing driven by continuous advancements in

sectors such as coatings, adhesives, sealants, and electronic materials. However, at present, its side product DMDVS does not have any specific industrial application, resulting in long-term storage and the risk of atmospheric release. On the other hand, sulfur has a high abundance on Earth, making it the 16<sup>th</sup> most abundant in the Earth's upper continental crust,<sup>5,8</sup> predominantly occurring as sulfide and sulfate minerals. Sulfur holds significant value in industry, agriculture, and materials science.<sup>9–11</sup> Meanwhile, elemental sulfur today is mostly derived as a byproduct from the petrochemical industry during the sulfur removal processes from crude oil and natural gas.<sup>12,13</sup> In 2021 alone, over 81 million tons of sulfur were produced across the globe,<sup>14</sup> surpassing its consumption in the production of sulfuric acid, fertilizers, and fungicides. The excess sulfur, stored as powder or bricks outdoors, presents potential environmental challenges that have yet to be fully addressed.<sup>8,14–16</sup>

Pyun and coworkers<sup>17</sup> pioneered inverse vulcanization, a method to utilize these two abundant low-value chemicals. Inverse vulcanization is a solvent-free reaction that produces a sulfur-rich functional polymer by radical polymerization between unsaturated organic crosslinkers and sulfur. Sulfur

<sup>a</sup>School of Physical Science and Technology, ShanghaiTech University, Shanghai 201210, P. R. China. E-mail: [jqj@shanghaitech.edu.cn](mailto:jjq@shanghaitech.edu.cn), [yanjj@shanghaitech.edu.cn](mailto:yanjj@shanghaitech.edu.cn)

<sup>b</sup>School of Life Science and Technology, ShanghaiTech University, Shanghai 201210, P. R. China

<sup>c</sup>Zhangjiang Laboratory, Shanghai 201210, P. R. China

†These authors contributed equally to this work.



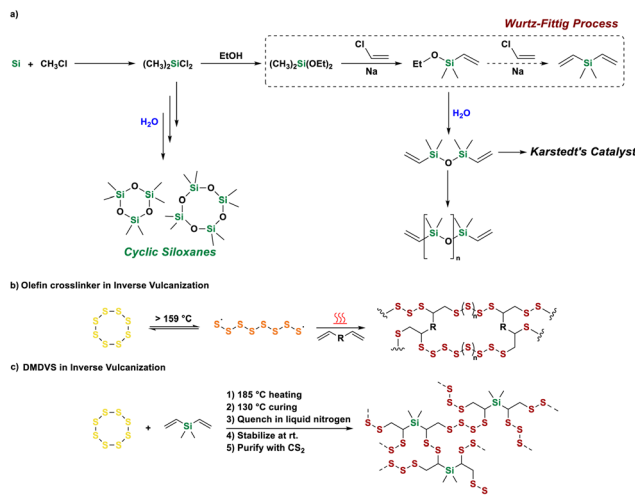
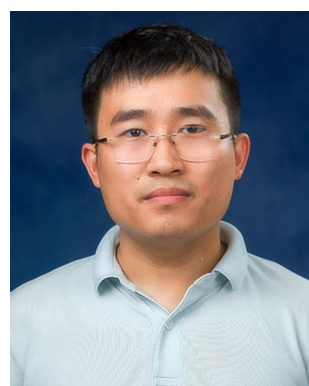


**Fig. 1** Overview of DMDVS and its inverse vulcanization. (a) Production of siloxanes and DVDSi in the silicone industry. (b) A general scheme of inverse vulcanization, where R indicates the core of small-molecule crosslinkers. (c) Proposed structure of poly(DMDVS-r-S) and key steps toward it.

melts and undergoes ring-opening to produce chain-end radicals over 159 °C that add to crosslinkers (Fig. 1b).<sup>18</sup> Since then, notable progress has been made in both the inverse vulcanization procedure and the applications of these unique sulfur-rich functional polymers. The range of organic crosslinkers explored for inverse vulcanization has expanded from synthetic feedstocks, such as 1,3-diisopropenylbenzene<sup>17,19,20</sup> and divinylbenzene,<sup>21,22</sup> to silicon-containing crosslinkers such as styreneethyltrimethoxysilane<sup>23</sup> and high-modulus reprographic silicone,<sup>24</sup> to bio-based resources such as limonene,<sup>25</sup> vegetable oils,<sup>26,27</sup> thioctic acid and its derivatives.<sup>28,29</sup> Currently, the primary methods for inverse vulcanization include heat activation,<sup>17,30</sup> diethyldithiocarbamate catalysis,<sup>30</sup> mechanochemical activation,<sup>31</sup> chemical vapor deposition,<sup>32,33</sup> photoactivation,<sup>34</sup> and anionic methods.<sup>35,36</sup> Beyond inverse



Jiajun Yan

Berkeley Lab until 2021, when he started his independent career at ShanghaiTech.

vulcanization, several novel approaches for sulfur valorization have emerged. Pyun and co-workers have employed sulfenyl chlorides to synthesize disulfide-linked polymers.<sup>37</sup> Chalker and co-workers introduced trisulfide electrochemical and photochemical initiation strategies for the preparation of poly(trisulfide) materials.<sup>38–40</sup> These sulfur-rich functional polymers can be utilized in various fields such as infrared optics,<sup>11,19,20,40–44</sup> antibacterial surfaces,<sup>45–48</sup> pollution remediation,<sup>25,31,47,49–51</sup> precious metal acquisition,<sup>30,39,52</sup> lithium–sulfur batteries,<sup>8,11,53–56</sup> bitumen-like materials,<sup>57</sup> high-refractive-index coatings,<sup>32,58</sup> and pressure-sensitive adhesives.<sup>18,28,59,60</sup>

Herein, we report a new sulfur-rich dynamic polymer network produced by inverse vulcanization of DMDVS, effectively upcycling these low-value industrial side streams into an advanced functional material with unprecedented thermo-responsive behavior. Unlike conventional inverse vulcanized networks, our polymer network exhibits unique dynamic behavior enabled by the distinctive molecular architecture of DMDVS, including extended polysulfide domains stabilized by the Si-based framework and temperature-dependent phase transitions. While being a viscous liquid at elevated temperature, it can be trapped in a gel state by rapid quenching. The network becomes unstable at room temperature with spontaneous elemental sulfur segregation through a solid–solid transition. Upon removal of the elemental sulfur, it transforms into a denser yet fully reprocessable elastomer. Remarkably, the resulting sulfur-rich film, serving as a packaging material, can improve the high-temperature performance of monolayer MoS<sub>2</sub> transistors by inhibiting sulfur vacancies in the latter.

## Results and discussion

### Material preparation

Based on previous studies,<sup>57,61–64</sup> we establish an optimized procedure for DMDVS inverse vulcanization, consisting of five key steps as depicted in Fig. 1c: (1) 185 °C reaction, (2) curing at 130 °C, (3) liquid nitrogen quenching, (4) room-temperature stabilization, and (5)  $\text{CS}_2$  (toxic) extraction. As demonstrated in a prior work,<sup>17</sup> effective inverse vulcanization requires homogeneously blending molten sulfur and a nonvolatile divinyl crosslinker at an elevated temperature to open  $\text{S}_8$  rings and facilitate sulfur radical addition to vinyl groups.<sup>65</sup> However, DMDVS, with a low boiling point of 82 °C, is immiscible with molten sulfur due to its rapid vaporization at >100 °C. To overcome this challenge, we used a sealed tall vial (Fig. S1) as a disposable reactor and condenser to house the reactants throughout the reaction.

The appearance of the mixture evolved throughout the reaction. It turned into a low viscosity orange liquid when initially heated to 185 °C, as shown in Fig. S2. After staying at 185 °C for 1 h, the system transformed into a pomegranate-red liquid with an increased viscosity. A curing step at 130 °C was implemented to allow thorough exchange and formation of the networks.<sup>61</sup> After the temperature was maintained at



130 °C for 24 h, the system evolved into a dark red liquid with higher viscosity and became almost black for 45 h. As we quenched that dark viscous liquid in liquid nitrogen, it turned into a metastable elastic gel (Fig. S2a and S3), which remained stable only below –5 °C (Fig. S4).

To distinguish the polymer networks prepared with different feeding ratios, we name them poly(DMDVS<sub>x</sub>-r-S<sub>y</sub>), where *x* and *y* are the weight fractions of the two reactants in tenths. The gel obtained by rapid quenching is denoted poly(DMDVS<sub>x</sub>-r-S<sub>y</sub>)-G. The metastable gel slowly became a rusty brown solid at room temperature (Fig. 1c and Fig. S2a). The solid, denoted poly(DMDVS<sub>x</sub>-r-S<sub>y</sub>)-S (Fig. S3), was stable at room temperature. If the cured polymer melt was cooled slowly from 130 °C, it formed the same solid.

As DMDVS is highly volatile at the reaction temperature, to exclude the possibility that what we observed was only the phase transition of sulfur,<sup>17</sup> we recorded the appearance changes of elemental sulfur subjected to the same treatment (Fig. S2b). The molten sulfur was much lighter in color and the sample restored the original appearance as a yellow powder as it returned to room temperature. This validated that poly(DMDVS<sub>x</sub>-r-S<sub>y</sub>) is distinct from elemental sulfur, while poly(DMDVS<sub>x</sub>-r-S<sub>y</sub>)-S is its stable form. We also found that increasing the DMDVS feed inhibited polymerization. Poly(DMDVS<sub>2</sub>-r-S<sub>8</sub>) showed unexpected swelling prior to curing (Fig. S2c), indicating that the intended polymerization was inhibited. Therefore, a 10% DMDVS feed was selected for further studies.

We examined the Si contents and glass transition temperatures (*T*<sub>g</sub>) of these polymers prepared under different conditions (Table 1) by inductively coupled plasma optical emission spectrometry (ICP-OES) and differential scanning calorimetry (DSC) to preliminarily understand their composition. Interestingly, ICP-OES results revealed that poly(DMDVS<sub>1</sub>-r-S<sub>9</sub>) contained a greater Si content than samples with a smaller or larger DMDVS feed. It was found that the silicon content has a negative correlation with reaction time but a positive correlation with curing time. Thus, the former contributed more to the evaporation as the latter helped with the incorporation.

As for *T*<sub>g</sub>, it has a negative correlation with curing time, indicating that curing promoted segment motion in the product, likely resulting from extended sulfur chains. The presence of a glass transition again proves that poly(DMDVS<sub>x</sub>-r-S<sub>y</sub>) is different from elemental sulfur, which exhibited two endothermic peaks at 107.8 and 113.6 °C (Fig. 2c).<sup>66</sup> Taking

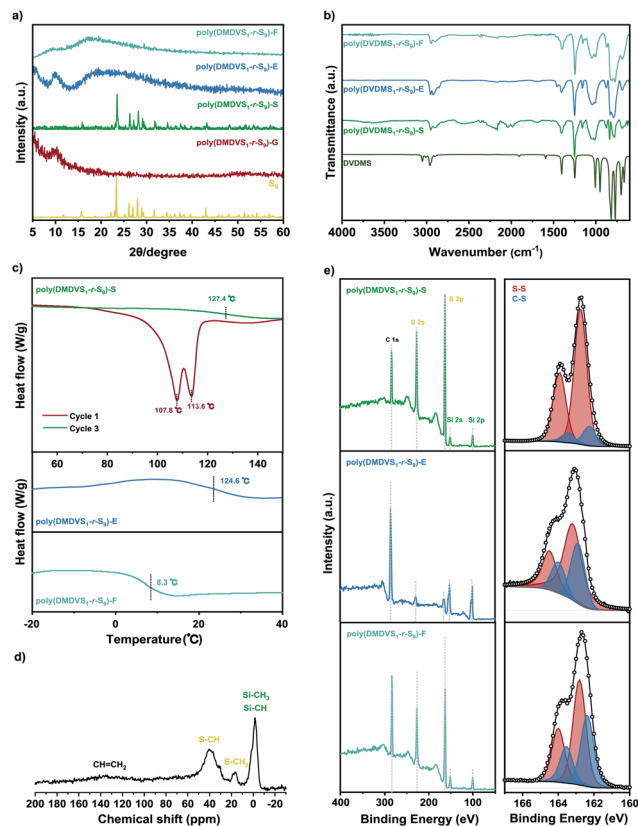


Fig. 2 Structural characterization of DMDVS-based inverse vulcanization polymers. (a) PXRD patterns of different poly(DMDVS<sub>1</sub>-r-S<sub>9</sub>) samples. (b) FT-IR spectra of poly(DMDVS<sub>1</sub>-r-S<sub>9</sub>) samples compared to DMDVS. (c) DSC curves. (d) <sup>13</sup>C solid-state NMR of poly(DMDVS<sub>1</sub>-r-S<sub>9</sub>)-S. (e) Full XPS surveys and deconvoluting spectra of S 2p.

**Table 1** Polymerization conditions and characteristics of copolymers

Polymer <sup>a</sup>	<i>m</i> <sub>0</sub> (DMDVS) : <i>m</i> <sub>0</sub> (S <sub>8</sub> ) (wt% : wt%)	Heating time (h)	Curing time (h)	Si content <sup>b</sup> (wt%)	<i>T</i> <sub>g</sub> , DSC <sup>c</sup> (°C)
Poly(DMDVS <sub>1.5</sub> -r-S <sub>8.5</sub> )-S	15 : 85	1	45	0.669 ± 0.051	125.4
Poly(DMDVS <sub>1</sub> -r-S <sub>9</sub> )-S	10 : 90	1	45	2.63 ± 0.21	127.4
Poly(DMDVS <sub>0.5</sub> -r-S <sub>9.5</sub> )-S	5 : 95	1	45	0.440 ± 0.023	114.0
Poly(DMDVS <sub>1</sub> -r-S <sub>9</sub> )-S	10 : 90	1	0	1.26 ± 0.35	134.2
Poly(DMDVS <sub>1</sub> -r-S <sub>9</sub> )-S	10 : 90	1	24	2.21 ± 0.33	129.8
Poly(DMDVS <sub>1</sub> -r-S <sub>9</sub> )-S	10 : 90	2	0	1.22 ± 0.13	134.2
Poly(DMDVS <sub>1</sub> -r-S <sub>9</sub> )-S	10 : 90	2	24	1.91 ± 0.18	131.0
Poly(DMDVS <sub>1</sub> -r-S <sub>9</sub> )-S	10 : 90	2	45	2.19 ± 0.23	124.8
Poly(DMDVS <sub>1</sub> -r-S <sub>9</sub> )-S	10 : 90	3	0	1.15 ± 0.09	132.9
Poly(DMDVS <sub>1</sub> -r-S <sub>9</sub> )-S	10 : 90	3	24	1.59 ± 0.18	128.8
Poly(DMDVS <sub>1</sub> -r-S <sub>9</sub> )-S	10 : 90	3	45	1.70 ± 0.12	128.4

<sup>a</sup> Reaction conditions: a 5 min quenching is applied after curing. <sup>b</sup> Average weight ratio (wt%) of silicon is determined by ICP-OES in 4 parallel tests, errors are the standard deviation of 4 samples and original data can be found in Table S1. <sup>c</sup> Extracted from the third cycle of DSC curves of each polymer. Full curves are available in Fig. S5.



the results in Table 1 into account, we selected poly(DMDVS<sub>1-r-S<sub>9</sub></sub>)-S from the second row with a 1-h reaction followed by 45 h of curing for the subsequent studies.

### Material characterization

In an unexpected turn of events, our powder X-ray diffraction (PXRD) examination of the solids revealed a pattern of poly(DMDVS<sub>1-r-S<sub>9</sub></sub>)-S closely aligned with that of S<sub>8</sub> (Fig. 2a). This finding contradicted our earlier verdict that poly(DMDVS<sub>x-r-S<sub>y</sub></sub>)-S differs from sulfur. Simultaneously, poly(DMDVS<sub>1-r-S<sub>9</sub></sub>)-G did not exhibit any discernible PXRD peak. This suggests that the sulfur signals in poly(DMDVS<sub>1-r-S<sub>9</sub></sub>)-S did not originate as a residue of the reactant. Instead, they were a result of transformations from poly(DMDVS<sub>1-r-S<sub>9</sub></sub>)-G when warmed to room temperature. Consequently, we postulate that a dynamic network with metastable long sulfur chains or rings was formed during the curing process, which was kinetically trapped by rapid quenching (Fig. 3a). As the temperature increased to ambient conditions, added thermal energy induced scission of the extended polysulfide chains, resulting in the formation of S<sub>8</sub> rings.

To verify that hypothesis, we first stored poly(DMDVS<sub>1-r-S<sub>9</sub></sub>)-G at -20 °C for over 6 months, observing no state change (Fig. S6). This proves that the transformation toward poly(DMDVS<sub>1-r-S<sub>9</sub></sub>)-S does need a sufficient energy input. As described above, the glass transition of poly(DMDVS<sub>x-r-S<sub>y</sub></sub>)-S was measured by DSC (Table 1 and Fig. S5) to provide evidence of its distinction from sulfur. However, pairs of apparent endothermic peaks related to the elemental sulfur were observed only in the first DSC cycles of all poly(DMDVS<sub>x-r-S<sub>y</sub></sub>)-S samples. For poly(DMDVS<sub>x-r-S<sub>y</sub></sub>)-S samples without curing, a new melting peak slightly lower than the original pair was observed in the second DSC cycle, indicating a less crystalline species related to the reactant. During the subsequent cycles, only glass transitions were detectable (Fig. 2c and Fig. S5). This means that although elemental sulfur did exist in poly

(DMDVS<sub>x-r-S<sub>y</sub></sub>)-S, the rate of its formation did not keep pace with the fast 10 °C min<sup>-1</sup> heating/cooling in the ensuing cycles. Hence, the rapid heating/cooling in DSC essentially reversed the transformation from poly(DMDVS<sub>x-r-S<sub>y</sub></sub>)-G to poly(DMDVS<sub>x-r-S<sub>y</sub></sub>)-S. Based on these experiments, we can firmly conclude that poly(DMDVS<sub>x-r-S<sub>y</sub></sub>)-S is a polymer network, wherein S<sub>8</sub> originates from rearrangement of longer sulfur chains.

With that in mind, we tried to extract elemental sulfur and any soluble molecules from poly(DMDVS<sub>1-r-S<sub>9</sub></sub>)-S (Fig. S7). However, all detected proton signals in the extracts were from the solvents implying the absence of soluble organic molecules. On the other hand, CS<sub>2</sub>, with its exceptional ability to dissolve elemental sulfur, was able to remove all S<sub>8</sub> molecules to yield a dark red elastomer, poly(DMDVS<sub>1-r-S<sub>9</sub></sub>)-E (Fig. S3), as evidenced by PXRD (Fig. 2a). Poly(DMDVS<sub>1-r-S<sub>9</sub></sub>)-E had a slightly lower *T<sub>g</sub>* (124.6 °C) than poly(DMDVS<sub>1-r-S<sub>9</sub></sub>)-S (Fig. 2c), indicating similar segment mobility. Meanwhile, it no longer had sulfur melting peaks in the first cycle (Fig. S5). Without any structural information from the extracts, we instead turn to solid-state <sup>13</sup>C nuclear magnetic resonance (NMR) and X-ray photoelectron spectroscopy (XPS) to gain an insight into the structure. We observed a sharp Si-C peak at ~0 ppm and a few broad S-C peaks between 10 and 60 ppm (Fig. 2d). Interestingly, a broad but weak vinyl bump at 130 ppm was also present. Poly(DMDVS<sub>1-r-S<sub>9</sub></sub>)-E showed almost identical <sup>13</sup>C NMR features (Fig. S8) but the Si-C peak splits into two. This is likely a result of improved resolution after S<sub>8</sub> removal. We observed characteristic XPS peaks of S 2s, S 2p, Si 2s, and Si 2p in both poly(DMDVS<sub>1-r-S<sub>9</sub></sub>)-S and poly(DMDVS<sub>1-r-S<sub>9</sub></sub>)-E (Fig. 2e). The reduced intensity of sulfur peaks in the full XPS surveys of poly(DMDVS<sub>1-r-S<sub>9</sub></sub>)-E further confirmed the removal of crystalline sulfur. Assuming that each C=C bond formed two C-S bonds, we were able to determine the sulfur rank (SR)<sup>33</sup> of poly(DMDVS<sub>1-r-S<sub>9</sub></sub>)-S based on eqn (1) derived in the SI and the silicon content measured by ICP-OES (Table 1).

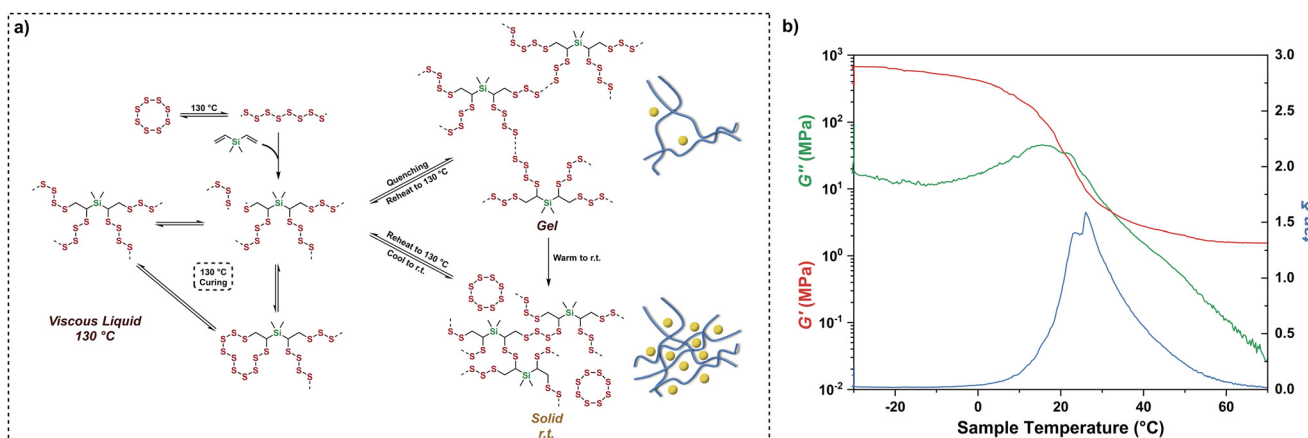


Fig. 3 Mechanical studies of poly(DMDVS<sub>1-r-S<sub>9</sub></sub>)-G and proposed mechanisms. (a) The proposed mechanism of the reaction between DMDVS and S<sub>8</sub> and the formation of different types of poly(DMDVS<sub>x-r-S<sub>y</sub></sub>). (b) DMA of poly(DMDVS<sub>1-r-S<sub>9</sub></sub>)-F. The specimen was cut into 8.0 mm × 35 mm × 0.10 mm (width × length × thickness).



$$SR = \frac{A_r(\text{Si}) - \omega_{\text{Si}} M_r(\text{DMDVS})}{2\omega_{\text{Si}} A_r(\text{S})} \quad (1)$$

where  $A_r(\text{Si})$  and  $A_r(\text{S})$  are the atomic masses of Si and S,  $M_r(\text{DMDVS})$  is the molar mass of DMDVS and  $\omega_{\text{Si}}$  is the Si content in Table 1, respectively.

This yields an SR of 14.9. Furthermore, by deconvoluting the S 2p doublets (Fig. 2e), we calculated an SR of 15.8 from eqn (2)<sup>33</sup> and Table S2, offering further consistency between the two methods.

$$SR = \frac{A_{\text{S-S}}}{A_{\text{C-S}}} \times 2 + 2 \quad (2)$$

where  $A_{\text{S-S}}$  and  $A_{\text{C-S}}$  are the areas of S-S and C-S signals in the deconvoluted S 2p doublet, respectively.

However, poly(DMDVS<sub>1-r-S<sub>9</sub></sub>)-E does not digest fully even under high-temperature microwave treatment. We instead determined the SR to be 4.5 by deconvoluting S 2p doublets in high-resolution XPS scans (Fig. 2e).<sup>33</sup> These findings again verify our hypothesis on poly(DMDVS<sub>1-r-S<sub>9</sub></sub>) transformations. Solubility tests further revealed that poly(DMDVS<sub>1-r-S<sub>9</sub></sub>)-E had good resistance to common solvents (Fig. S9).

Fourier transform infrared (FT-IR) spectra (Fig. 2b) showed an absorption peak at 1157 cm<sup>-1</sup> corresponding to the C-S stretching vibration in poly(DMDVS<sub>1-r-S<sub>9</sub></sub>)-S and poly(DMDVS<sub>1-r-S<sub>9</sub></sub>)-E, while the peaks related to -CH=CH<sub>2</sub> were absent. Peaks at 1406 cm<sup>-1</sup> and 1250 cm<sup>-1</sup> corresponding to Si-C bonds were still present in the polymer but with a shift in their intensity ratio from the DMDVS monomer. These observations mean that during the reaction, vinyl groups were mostly converted to the C-S species albeit its detection by highly sensitive solid-state NMR acquisition. Meanwhile, the 400 cm<sup>-1</sup> S-S stretching was too weak to be observed.<sup>18,41,64,67</sup>

Due to its lack of stability, poly(DMDVS<sub>1-r-S<sub>9</sub></sub>)-G is particularly difficult to characterize. We stored the sample in liquid nitrogen before performing the rheology test on it at -10 °C.  $G''$  was slightly larger than  $G'$  over a range from 0.1 to 628.3 rad s<sup>-1</sup> (100 Hz), until a crossover occurred at 421.6 rad s<sup>-1</sup> (67 Hz), while  $\tan \delta$  was nearly constant over a range from 0.1 to 23.7 rad s<sup>-1</sup>, indicating a loose network with long sulfur chains between crosslinking points (Fig. S10a). Fig. S10b shows that poly(DMDVS<sub>1-r-S<sub>9</sub></sub>)-G can sustain a small strain between the plates before breakage, when  $G''$  dropped below  $G'$  as the sulfur chains fractured.

Based on the results above, we conclude that the copolymerization process produces a temperature-responsive dynamic polymer network, poly(DMDVS<sub>x-r-S<sub>y</sub></sub>). We propose a mechanism of the reaction between DMDVS and S<sub>8</sub>, as illustrated in Fig. 3a. Initially, high temperature (185 °C) induces the cleavage of S-S in S<sub>8</sub> to generate sulfur radicals like other heat-activated inverse vulcanization processes.<sup>17,68,69</sup> This is followed by bulk polymerization, leading to the formation of the sulfur-rich network with long sulfur chains or large sulfur rings. Rapid quenching in liquid nitrogen preserves these high-temperature structures, while low temperature (-20 °C, *e.g.*) storage kinetically traps the segment motion to retain this

structure. At room temperature, the thermodynamically labile long sulfur chains undergo S-S bond cleavage and recombination to form a more stable short-chain network alongside S<sub>8</sub> interspersed in the network. Free S<sub>8</sub> can reintegrate into the polymer network by heating, as observed in DSC (Fig. 2c).

Our density functional theory (DFT) calculations by considering a simplified model of poly(DMDVS<sub>x-r-S<sub>y</sub></sub>) further affirm the proposed mechanism, featuring a minimum at SR = 6 in the calculated energy landscape (Fig. S11 and S12), in agreement with the experimentally determined SR of poly(DMDVS<sub>1-r-S<sub>9</sub></sub>)-E. It is anticipated that the DMDVS crosslinkers reduce the packing density of long sulfur chains, leading to prominent metastability in the high-SR case, while a moderate SR (*e.g.*, 4-6) achieves balance between ring tension and chain instability, contributing to the global formation energy minima. Such structural traits bestow the dynamic and temperature-responsive feature to the poly(DMDVS<sub>x-r-S<sub>y</sub></sub>) material.

The random physical forms of as-prepared poly(DMDVS<sub>1-r-S<sub>9</sub></sub>)-E posed challenges for subsequent studies. Meanwhile, the dynamic covalent characteristic makes this polymer reprocesable. Therefore, we hot-pressed poly(DMDVS<sub>1-r-S<sub>9</sub></sub>)-E at 120 °C and 2 MPa for 3 min after 3 min of preheating. Poly(DMDVS<sub>1-r-S<sub>9</sub></sub>)-E exhibited excellent malleability (Fig. S13). We denote the polymer film obtained over 3 hot-press cycles as poly(DMDVS<sub>1-r-S<sub>9</sub></sub>)-F. The film had an identical FT-IR spectrum to poly(DMDVS<sub>1-r-S<sub>9</sub></sub>)-E but showed different PXRD patterns, glass transition temperature, and XPS (Fig. 2). Some lower angle features seen in poly(DMDVS<sub>1-r-S<sub>9</sub></sub>)-E and poly(DMDVS<sub>1-r-S<sub>9</sub></sub>)-G vanished after pressing, indicating a loss of long period orders, probably related to clusters. The glass transition temperature was over 100 °C lower while sulfur melting was still absent in the first cycle (Fig. S5). This significant decrease of  $T_g$  after hot-pressing suggested that the tight network in poly(DMDVS<sub>1-r-S<sub>9</sub></sub>)-E rearranged into a loose network in poly(DMDVS<sub>1-r-S<sub>9</sub></sub>)-F with the stress in the network relaxed as suggested in earlier reports. Bischoff *et al.* classified inverse vulcanized polymers as covalent adaptable networks (CANs), which exhibit thermoset characteristics with exchangeable bonds.<sup>22</sup> The application of heat facilitates exchange within CANs, altering their topology and rheological properties, thus enabling creep recovery and stress relaxation (Fig. S14). Rheological studies in previous work provide further evidence of the active dynamic covalent process of S-S bonds in inverse vulcanized polymers over 100 °C.<sup>22,70</sup> XPS showed stronger sulfur peaks indicating more sulfur at the surface, but there was only a subtle increase in SR to 4.9 (5.3 calculated from eqn (1) and Table S1), proving that the hot-press did not significantly alter the average length of sulfur chains.

We assessed the viscoelastic properties of the film by using dynamic mechanical analysis (DMA). Overall, the poly(DMDVS<sub>1-r-S<sub>9</sub></sub>)-F film behaved as a lightly crosslinked elastomer. At lower temperature, its  $G'$  was larger than  $G''$ , and a glassy plateau with a  $G'$  close to 3 GPa was observed.  $G'$  started to drop above 0 °C as the film entered its glass transition, followed by a rubbery plateau with a storage modulus of several MPa beyond 40 °C. The measured  $T_g$  (~25 °C) was higher than



the DSC result (8.3 °C) (Fig. 3b). To investigate the high-temperature rheological behavior of poly(DMDVS<sub>1-r</sub>-S<sub>9</sub>)-F, we conducted rheological measurements at 150 °C. In the terminal region,  $G''$  exceeded  $G'$  over a frequency range of  $6.28 \times 10^{-3}$  to 100 rad s<sup>-1</sup>, with a crossover observed near 0.1 rad s<sup>-1</sup> (Fig. S10c). Comparative analysis of Fig. 3b and Fig. S10a reveals that both  $G'$  and  $G''$  values for poly(DMDVS<sub>1-r</sub>-S<sub>9</sub>)-F at -10 °C are greater than those of poly(DMDVS<sub>1-r</sub>-S<sub>9</sub>)-G. Meanwhile, poly(DMDVS<sub>1-r</sub>-S<sub>9</sub>)-G showed a  $G''$  higher than its  $G'$ , while poly(DMDVS<sub>1-r</sub>-S<sub>9</sub>)-F exhibited  $G''$  exceeding  $G'$ . This suggested a denser network structure with shorter sulfur chain segments between crosslink points, which was different from poly(DMDVS<sub>1-r</sub>-S<sub>9</sub>)-G formed in poly(DMDVS<sub>1-r</sub>-S<sub>9</sub>)-F. The rheological properties of these two samples were consistent with their morphologies.

The thermal processability and its room temperature glass transition behavior make the poly(DMDVS<sub>1-r</sub>-S<sub>9</sub>)-F film suitable for solvent-free coating applications. The film demonstrated moderate hydrophobicity, as indicated by a water contact angle of 94.4° (Fig. S15). To assess its in-service stability, the sample was subjected to continuous heating at 150 °C, the highest operational temperature, in a nitrogen atmosphere, revealing a sustained sulfur release over 96 h, which was favorable for filling the sulfur vacancies in the intended application (Fig. S16).

## Material applications

Two-dimensional (2D) materials, exemplified by graphene and monolayer MoS<sub>2</sub>, have emerged as promising candidates for next-generation electronics due to their ultrathin bodies, dangling bond-free interfaces, and tunable band structures.<sup>71-73</sup> However, MoS<sub>2</sub>-based devices face operational challenges under elevated temperature conditions. When exposed to temperatures approaching 100 °C, sulfur vacancies (SVs) in MoS<sub>2</sub> are thermally generated,<sup>74,75</sup> creating charge trapping centers.<sup>76-79</sup> These SVs collectively degrade electrical stability, manifesting as both hysteresis window broadening and sub-threshold swing (SS) degradation.<sup>80</sup>

As illustrated in Fig. 4a and b, the polymer-encapsulated MoS<sub>2</sub> field-effect transistor (FET) architecture can effectively address this challenge. Fig. 4c and d show the transfer curves of MoS<sub>2</sub> and poly(DMDVS<sub>1-r</sub>-S<sub>9</sub>)-F/MoS<sub>2</sub> FETs, respectively, under cyclic  $V_{bg}$  sweeps between -100 V and +80 V. For the bare MoS<sub>2</sub> device, the hysteresis window exhibits a substantial increase (Fig. 4c) from 4 V at 25 °C to 38 V at 150 °C. Poly(DMDVS<sub>1-r</sub>-S<sub>9</sub>)-F encapsulation effectively suppresses this thermally amplified hysteresis (Fig. 4d), reducing the hysteresis window from 38 V to 20 V. The suppression ratio, calculated using eqn (3) below, reaches 47% at 150 °C (Fig. 4e).

$$\text{Suppression ratio} = \left(1 - \frac{\Delta V_{\text{polymer}}}{\Delta V_{\text{MoS}_2}}\right) \times 100\% \quad (3)$$

By contrast, the suppression ratios for sulfur powder and poly(DMDVS<sub>1-r</sub>-S<sub>9</sub>)-S are 5% and 36% (Fig. 4e and Fig. S17), respectively. This inefficiency arises from their side effects: physical adsorption of powders creates interface nonuniform-

ity, which enlarges the baseline hysteresis even at room temperature (Fig. 4e).<sup>76</sup> Notably, poly(DMDVS<sub>1-r</sub>-S<sub>9</sub>)-F encapsulation does not induce additional hysteresis at 25 °C, confirming that its vacancy-passivating function is thermally activated and interface-protective. These results experimentally confirm the inhibitory effect of poly(DMDVS<sub>1-r</sub>-S<sub>9</sub>)-F on hysteresis window broadening of monolayer MoS<sub>2</sub> FETs at elevated temperatures.

In parallel with the hysteresis analysis, the temperature-dependent increase in SS exhibits a direct proportionality to SV concentration ( $\Delta SS \propto \Delta N_{\text{SVs}}$ ),<sup>81,82</sup> as derived in the SI. To elucidate the quantitative relationship between sulfur vacancy concentration and SS degradation in MoS<sub>2</sub> FETs, we derived an analytical model based on semiconductor electrostatics (eqn (S1)-(S9)).<sup>83</sup> In this model, SS is expressed as a function of the depletion and oxide capacitances, with the depletion capacitance being influenced by the effective doping concentration ( $N_{\text{eff}}$ ). Since thermally generated  $\Delta N_{\text{SVs}}$  act as donor-like defects, they increase  $N_{\text{eff}}$ , leading to a measurable rise in SS. Assuming a proportional relationship between  $\Delta N_{\text{SVs}}$  and  $\Delta N_{\text{eff}}$ , we arrived at a simplified expression showing that  $\Delta SS$  is directly proportional to  $\Delta N_{\text{SVs}}$ . As summarized in Table S3,  $\Delta SS$  at 150 °C is most severe in the bare MoS<sub>2</sub> FET (+2.22 V dec<sup>-1</sup>, 84% SV increase), corresponding to thermally activated sulfur volatilization. The poly(DMDVS<sub>1-r</sub>-S<sub>9</sub>)-F/MoS<sub>2</sub> FET shows a mitigated  $\Delta SS$  of +0.99 V dec<sup>-1</sup> (21% SV increase), validating its inhibitory effect against sulfur loss. Meanwhile, sulfur powder-coated and poly(DMDVS<sub>1-r</sub>-S<sub>9</sub>)-S-encapsulated FETs exhibit intermediate SV suppression ( $\Delta N_{\text{SVs}} = 59\%$  and 46%, respectively), limited by incomplete defect passivation due to insufficient interfacing. To describe the temperature-dependent charge trapping/de-trapping dynamics at the heterointerface, we have systematically constructed correlated hysteresis models accompanied by the corresponding energy band diagrams (Fig. 4f).<sup>78,79</sup> At room temperature (25 °C), the hysteresis window in the MoS<sub>2</sub> FET is nearly negligible under vacuum (Fig. 4c and e), confirming the intrinsically low SVs in pristine MoS<sub>2</sub> (Fig. S18).<sup>76,77</sup> Therefore, electrons are directly injected into the conduction band of MoS<sub>2</sub> under a positive gate voltage, whereas they are reversibly withdrawn under negative gate bias, resulting in a negligibly small hysteresis window, as shown in Fig. 4f(i).

Under elevated temperature (e.g., 150 °C), sulfur atoms in the MoS<sub>2</sub> lattice acquire sufficient thermal energy to dissociate from their crystallographic positions, resulting in an increase in SVs.<sup>74,75</sup> These SVs introduce deep-level donor states below the conduction band edge (Fig. 4f(ii)),<sup>79</sup> which act as dynamic charge trapping centers, resulting in pronounced hysteresis during gate voltage sweeps (Fig. 4c and e).<sup>77</sup> Under positive gate bias, electron trapping at vacancy sites increases the threshold voltage ( $V_{\text{th}}$ ), whereas electron de-trapping under negative gate bias reduces  $V_{\text{th}}$ . This mechanism leads to a clockwise hysteresis in agreement with prior reports.<sup>76,77</sup>

Our experimental results have shown that the sulfur-rich poly(DMDVS<sub>1-r</sub>-S<sub>9</sub>)-F encapsulation layer undergoes thermally induced chain scission at elevated temperatures, releasing



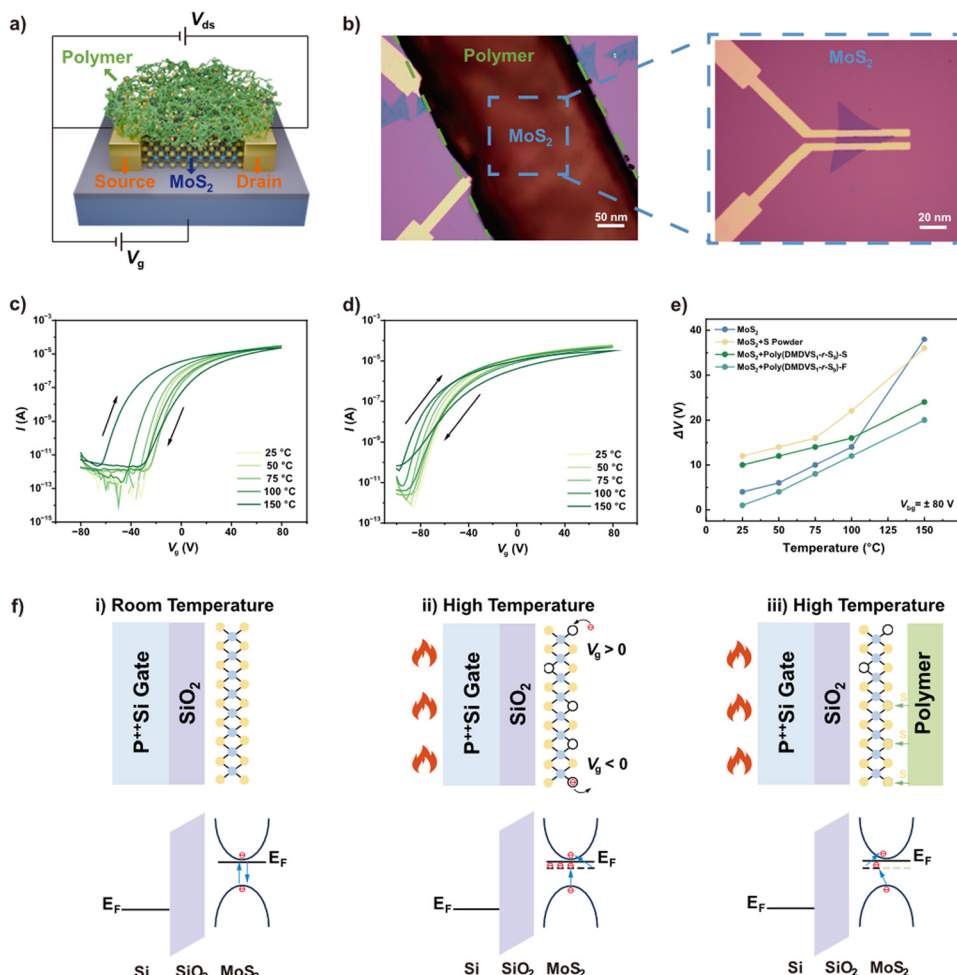


**Fig. 4** Electrical characteristics of the MoS<sub>2</sub>/poly(DMDVS<sub>1</sub>-r-S<sub>9</sub>)-F device. (a) Scheme and (b) optical micrograph of the MoS<sub>2</sub>/poly(DMDVS<sub>1</sub>-r-S<sub>9</sub>)-F device. MoS<sub>2</sub> and poly(DMDVS<sub>1</sub>-r-S<sub>9</sub>)-F were outlined by the blue and green dashed lines, respectively. Transfer curves of the MoS<sub>2</sub> FETs (c) without and (d) with poly(DMDVS<sub>1</sub>-r-S<sub>9</sub>)-F measured across varying temperatures under vacuum.  $V_g$  from  $-100$  to  $80$  V back and forth at  $V_{ds} = 1$  V. (e) Extracted hysteresis window as a function of temperature incorporating various sulfur-containing materials. (f) Proposed mechanisms for hysteresis alongside the corresponding band diagrams: thermally activated SVs act as electron trapping/de-trapping centers in MoS<sub>2</sub>, whereas sulfur moieties in the polymer partially passivate these SVs, thereby suppressing the hysteresis window at elevated temperatures.

sulfur-containing moieties that coordinate with under-coordinated Mo atoms at the MoS<sub>2</sub> interface (Fig. 4F(iii)). This dynamic passivation process suppresses SV formation below a critical threshold, stabilizing the hysteresis window and sub-threshold swing. This approach hence unlocks the application potential of two-dimensional sulfide materials in high-temperature electronics, harnessing the sustained sulfur release property of the dynamic sulfur-rich network.

## Conclusions

In summary, this work has demonstrated a waste-to-value transformation of sulfur-rich dynamic polymer networks from the combination of two considerable forms of industrial waste: dimethyldivinyldisilane and elemental sulfur. Elevated temperatures prompt the S<sub>8</sub> ring to open, resulting in radical polymerization in a viscous fluid that solidifies upon cooling, forming

an elastic gel when the liquid mixture is rapidly quenched in liquid nitrogen and stored at low temperatures. Warming this gel triggers decomposition that leaves behind elemental sulfur and a denser network. Following the removal of such elemental sulfur, the residual sulfur-rich network can be molded into films, showing potential as a protective coating for monolayer MoS<sub>2</sub> transistors. This coating as a sulfur reservoir significantly reduces the switching hysteresis of the device by 47% at 150 °C, thanks to the sustained sulfur release of the polymer that passivates the otherwise abundant sulfur vacancies in MoS<sub>2</sub>. The inherent dual-vinyl functionalities of dimethyldivinyldisilane endow it with immense potential in constructing functional polymers. This work plants the seed of possibility in transforming low-value industrial waste into functional materials for future advancements, thereby advocating for an increased focus on the value-added applications of waste chemicals. We envision this study opening another path towards achieving sustainability.

## Author contributions

Conceptualization, J. Y., Q. J., and Z. W.; methodology, Z. W., J. Y., Q. J., Y. L., and Y. Q.; validation, J. Y., Q. J., and Z. W.; formal analysis, Z. W., J. Y., Y. Q., and Q. J.; investigation, Z. W., Y. Q., Z. C., H. H., Y. S., X. L., Y. Y., and Y. L.; resources, J. Y. and Q. J.; data curation, Z. W., Y. Q., J. Y., and Q. J.; writing – original draft, Z. W., J. Y., and Y. Q.; writing – review & editing, J. Y. and Q. J.; visualization, Z. W., Y. Q., and Y. S.; supervision, J. Y., Q. J., and H. Z.; project administration, J. Y., Q. J., and H. Z.; and funding acquisition, J. Y., Q. J., H. Z., and H. H.

## Conflicts of interest

Part of the results have been filed in a patent (CN118930861B) by ShanghaiTech University with J. Y., Z. W., and Z. C. as inventors. Zhejiang Jiancheng New Materials Co., Ltd, a material donor, may potentially benefit from the findings.

## Data availability

The data supporting the findings of this study are available from the corresponding author upon reasonable request.

Supplementary information (SI): all experimental data, including experimental methods, raw measurements, characterization results and calculations. See DOI: <https://doi.org/10.1039/d5gc02864g>.

## Acknowledgements

This work is financially supported by ShanghaiTech University *via* the start-up grant (J. Y.) and the Double First-Class Initiative Fund (H. H.), the Science and Technology Commission of Shanghai Municipality *via* Grant No. 22YF1428200 (J. Y.), and the National Natural Science Foundation of China *via* Grant No. 22401188 (J. Y.) and 22205142 (Q. J.). We thank Zhejiang Jiancheng New Materials Co., Ltd for their kind donation of dimethyldivinylsilane. We thank Prof. Yingbo Zhao for providing access to the DMA and Prof. Yijun Zheng for providing access to the rheometer. We also acknowledge support from the Analytical Instrumentation Center (Contract No. SPST-AIC10112914) at the School of Physical Science and Technology, ShanghaiTech University.

## References

- 1 W. C. Schumb, J. Ackerman Jr. and C. M. Saffer Jr., *J. Am. Chem. Soc.*, 1938, **60**, 2486–2488.
- 2 M. Kanazashi, *Bull. Chem. Soc. Jpn.*, 1953, **26**, 493–496.
- 3 Y. Yang, *China Pat.*, CN101792459, 2010, Zhejiang Jiahui New Material Co., Ltd.
- 4 B. He, Y. Yang and Z. Wen, *China Pat.*, CN112625058, 2021, Zhejiang Jiahui New Material Co., Ltd.
- 5 A. A. Yaroshevsky, *Geochem. Int.*, 2006, **44**, 48–55.
- 6 A. M. Tondreau, C. C. H. Atienza, K. J. Weller, S. A. Nye, K. M. Lewis, J. G. P. Delis and P. J. Chirik, *Science*, 2012, **335**, 567–570.
- 7 T. K. Meister, K. Riener, P. Gigler, J. Stohrer, W. A. Herrmann and F. E. Kühn, *ACS Catal.*, 2016, **6**, 1274–1284.
- 8 J. J. Griebel, R. S. Glass, K. Char and J. Pyun, *Prog. Polym. Sci.*, 2016, **58**, 90–125.
- 9 D. A. Boyd, *Angew. Chem., Int. Ed.*, 2016, **55**, 15486–15502.
- 10 Y. Zhang, R. S. Glass, K. Char and J. Pyun, *Polym. Chem.*, 2019, **10**, 4078–4105.
- 11 T. Lee, P. T. Dirlam, J. T. Njardarson, R. S. Glass and J. Pyun, *J. Am. Chem. Soc.*, 2022, **144**, 5–22.
- 12 R. J. Angelici, *Acc. Chem. Res.*, 1988, **21**, 387–394.
- 13 T. Rauchfuss, *Nat. Chem.*, 2011, **3**, 648–648.
- 14 C. King-Poole and H. Thérien-Aubin, *Adv. Funct. Mater.*, 2024, **34**, 2405608.
- 15 J. Lim, J. Pyun and K. Char, *Angew. Chem., Int. Ed.*, 2015, **54**, 3249–3258.
- 16 T. Tian, R. Hu and B. Z. Tang, *J. Am. Chem. Soc.*, 2018, **140**, 6156–6163.
- 17 W. J. Chung, J. J. Griebel, E. T. Kim, H. Yoon, A. G. Simmonds, H. J. Ji, P. T. Dirlam, R. S. Glass, J. J. Wie, N. A. Nguyen, B. W. Guralnick, J. Park, Á. Somogyi, P. Theato, M. E. Mackay, Y.-E. Sung, K. Char and J. Pyun, *Nat. Chem.*, 2013, **5**, 518–524.
- 18 J. Fan, C. Ju, S. Fan, X. Li, Z. Zhang and N. Hadjichristidis, *Angew. Chem., Int. Ed.*, 2025, **64**, e202418764.
- 19 J. J. Griebel, N. A. Nguyen, S. Namnabat, L. E. Anderson, R. S. Glass, R. A. Norwood, M. E. Mackay, K. Char and J. Pyun, *ACS Macro Lett.*, 2015, **4**, 862–866.
- 20 T. S. Kleine, N. A. Nguyen, L. E. Anderson, S. Namnabat, E. A. LaVilla, S. A. Showghi, P. T. Dirlam, C. B. Arrington, M. S. Manchester, J. Schwiegerling, R. S. Glass, K. Char, R. A. Norwood, M. E. Mackay and J. Pyun, *ACS Macro Lett.*, 2016, **5**, 1152–1156.
- 21 S. Diez, A. Hoefling, P. Theato and W. Pauer, *Polymers*, 2017, **9**, 59.
- 22 D. J. Bischoff, T. Lee, K.-S. Kang, J. Molineux, W. O. Paker, J. Pyun and M. E. Mackay, *Nat. Commun.*, 2023, **14**, 7553.
- 23 J. M. Scheiger, C. Direksilp, P. Falkenstein, A. Welle, M. Koenig, S. Heissler, J. Matysik, P. A. Levkin and P. Theato, *Angew. Chem., Int. Ed.*, 2020, **59**, 18639–18645.
- 24 M. Rokni, K. W. Park, W. H. Leung, Z. Zujovic and E. M. Leitao, *Mater. Adv.*, 2024, **5**, 5433–5441.
- 25 M. P. Crockett, A. M. Evans, M. J. H. Worthington, I. S. Albuquerque, A. D. Slattery, C. T. Gibson, J. A. Campbell, D. A. Lewis, G. J. L. Bernardes and J. M. Chalker, *Angew. Chem., Int. Ed.*, 2016, **55**, 1714–1718.
- 26 J. Cubero-Cardoso, A. A. Cuadri, F. G. Fermoso, J. E. Martín-Alfonso and J. Urbano, *ACS Appl. Polym. Mater.*, 2022, **4**, 3667–3675.



27 A. Hoefling, Y. J. Lee and P. Theato, *Macromol. Chem. Phys.*, 2017, **218**, 1600303.

28 Y. Deng, Z. Huang, B. L. Feringa, H. Tian, Q. Zhang and D.-H. Qu, *Nat. Commun.*, 2024, **15**, 3855.

29 C.-Y. Shi, X.-P. Zhang, Q. Zhang, M. Chen, H. Tian and D.-H. Qu, *Chem. Sci.*, 2024, **15**, 17460–17468.

30 X. Wu, J. A. Smith, S. Petcher, B. Zhang, D. J. Parker, J. M. Griffin and T. Hasell, *Nat. Commun.*, 2019, **10**, 647.

31 P. Yan, W. Zhao, F. McBride, D. Cai, J. Dale, V. Hanna and T. Hasell, *Nat. Commun.*, 2022, **13**, 4824.

32 D. H. Kim, W. Jang, K. Choi, J. S. Choi, J. Pyun, J. Lim, K. Char and S. G. Im, *Sci. Adv.*, 2020, **6**, eabb5320.

33 K. Choi, W. Jang, W. Lee, J. S. Choi, M. Kang, J. Kim, K. Char, J. Lim and S. G. Im, *Macromolecules*, 2022, **55**, 7222–7231.

34 J. Jia, J. Liu, Z.-Q. Wang, T. Liu, P. Yan, X.-Q. Gong, C. Zhao, L. Chen, C. Miao, W. Zhao, S. Cai, X.-C. Wang, A. I. Cooper, X. Wu, T. Hasell and Z.-J. Quan, *Nat. Chem.*, 2022, **14**, 1249–1257.

35 H. Yang, J. Huang, Y. Song, H. Yao, W. Huang, X. Xue, L. Jiang, Q. Jiang, B. Jiang and G. Zhang, *J. Am. Chem. Soc.*, 2023, **145**, 14539–14547.

36 H. Yang, J. Zhang, W. Huang and G. Zhang, *Angew. Chem., Int. Ed.*, 2025, **64**, e202414244.

37 K.-S. Kang, C. Olikagu, T. Lee, J. Bao, J. Molineux, L. N. Holmen, K. P. Martin, K.-J. Kim, K. H. Kim, J. Bang, V. K. Kumirov, R. S. Glass, R. A. Norwood, J. T. Njardarson and J. Pyun, *J. Am. Chem. Soc.*, 2022, **144**, 23044–23052.

38 J. M. M. Pople, T. P. Nicholls, L. N. Pham, W. M. Bloch, L. S. Lisboa, M. V. Perkins, C. T. Gibson, M. L. Coote, Z. Jia and J. M. Chalker, *J. Am. Chem. Soc.*, 2023, **145**, 11798–11810.

39 M. Mann, T. P. Nicholls, H. D. Patel, L. S. Lisboa, J. M. M. Pople, L. N. Pham, M. J. H. Worthington, M. R. Smith, Y. Yin, G. G. Andersson, C. T. Gibson, L. J. Esdaile, C. E. Lenehan, M. L. Coote, Z. Jia and J. M. Chalker, *Nat. Sustain.*, 2025, 947–956.

40 S. J. Tokin, H. D. Patel and J. M. Chalker, ChemRxiv, 2025, preprint, DOI: [10.26434/chemrxiv-2025-wd224-v2](https://doi.org/10.26434/chemrxiv-2025-wd224-v2).

41 J. J. Griebel, S. Namnabat, E. T. Kim, R. Himmelhuber, D. H. Moronta, W. J. Chung, A. G. Simmonds, K.-J. Kim, J. van der Laan, N. A. Nguyen, E. L. Dereniak, M. E. Mackay, K. Char, R. S. Glass, R. A. Norwood and J. Pyun, *Adv. Mater.*, 2014, **26**, 3014–3018.

42 Y. Wuliu, W. Dong, G. Huang, H. Xie, P. Yao, J. Tan, K. Mu, Z. Zhang, Y. Chen, M. Wang, L. Tian, C. Zhu and J. Xu, *Angew. Chem., Int. Ed.*, 2025, **64**, e202419446.

43 J. Pyun and R. A. Norwood, *Prog. Polym. Sci.*, 2024, **156**, 101865.

44 J. Molineux, T. Lee, K. J. Kim, K.-S. Kang, N. P. Lyons, A. Nishant, T. S. Kleine, S. W. Durfee, J. Pyun and R. A. Norwood, *Adv. Opt. Mater.*, 2024, **12**, 2301971.

45 Z. Deng, A. Hoefling, P. Théato and K. Lienkamp, *Macromol. Chem. Phys.*, 2018, **219**, 1700497.

46 R. A. Dop, D. R. Neill and T. Hasell, *Biomacromolecules*, 2021, **22**, 5223–5233.

47 X. Deng, R. A. Dop, D. Cai, D. R. Neill and T. Hasell, *Adv. Funct. Mater.*, 2024, **34**, 2311647.

48 S. K. Wijeyatunga, P. Y. Saucedo-Oloño, N. L. Kapuge Dona, B. G. S. Guinati, K. M. Derr, K. A. Tisdale, A. D. Smith, A. G. Tennyson and R. C. Smith, *Molecules*, 2025, **30**, 1614.

49 T. Hasell, D. J. Parker, H. A. Jones, T. McAllister and S. M. Howdle, *Chem. Commun.*, 2016, **52**, 5383–5386.

50 M. J. H. Worthington, R. L. Kucera and J. M. Chalker, *Green Chem.*, 2017, **19**, 2748–2761.

51 D. J. Parker, S. T. Chong and T. Hasell, *RSC Adv.*, 2018, **8**, 27892–27899.

52 J. Rollins, C. B. Call, D. Herrera and C. L. Jenkins, *ACS Appl. Polym. Mater.*, 2025, **7**, 8529–8537.

53 A. G. Simmonds, J. J. Griebel, J. Park, K. R. Kim, W. J. Chung, V. P. Oleshko, J. Kim, E. T. Kim, R. S. Glass, C. L. Soles, Y.-E. Sung, K. Char and J. Pyun, *ACS Macro Lett.*, 2014, **3**, 229–232.

54 J. W. Choi and D. Aurbach, *Nat. Rev. Mater.*, 2016, **1**, 16013.

55 L. Zhao, F. Qiu, X. Deng, Y. Huang, Y. Li, C. Zhao, W. Ren, C. Zou, X. Li, M. Wang and Y. Lin, *ACS Appl. Energy Mater.*, 2022, **5**, 7617–7626.

56 M. Wang, Z. Bai, T. Yang, C. Nie, X. Xu, Y. Wang, J. Yang, S. Dou and N. Wang, *Adv. Energy Mater.*, 2022, **12**, 2201585.

57 K.-X. Hou, P.-C. Zhao, L. Duan, M. Fan, P. Zheng and C.-H. Li, *Adv. Funct. Mater.*, 2023, **33**, 2306886.

58 X. Qian, *ACS Omega*, 2025, **10**, 3953–3959.

59 C. Herrera, K. J. Ysinga and C. L. Jenkins, *ACS Appl. Mater. Interfaces*, 2019, **11**, 35312–35318.

60 S. J. Tonkin, C. T. Gibson, J. A. Campbell, D. A. Lewis, A. Karton, T. Hasell and J. M. Chalker, *Chem. Sci.*, 2020, **11**, 5537–5546.

61 N. Han, W. Cho, J. H. Hwang, S. Won, D.-G. Kim and J. J. Wie, *Polym. Chem.*, 2023, **14**, 943–951.

62 B. Zheng, L. Zhong, X. Wang, P. Lin, Z. Yang, T. Bai, H. Shen and H. Zhang, *Nat. Commun.*, 2024, **15**, 5507.

63 T. Sehn, J. Fanelli, L. Wahl and M. A. R. Meier, *RSC Sustainability*, 2025, **3**, 291–299.

64 M. Vera-Tuset, R. Mas-Ballesté, I. Cuadrado, A. Moya and S. Bruña, *Polym. Chem.*, 2024, **15**, 1015–1025.

65 V. B. Purohit, M. Pięta, J. Pietrasik and C. M. Plummer, *Polym. Chem.*, 2022, **13**, 4858–4878.

66 L. Zhang, Y. Ren, X. Liu, F. Han, K. Evans-Lutterodt, H. Wang, Y. He, J. Wang, Y. Zhao and W. Yang, *Sci. Rep.*, 2018, **8**, 4558.

67 K. W. Park, E. A. Tafili, F. Fan, Z. Zujovic and E. M. Leitao, *Polym. Chem.*, 2022, **13**, 4717–4726.

68 R. S. Glass, in *Sulfur Chemistry*, ed. X. Jiang, Springer International Publishing, Gewerbestrasse, Cham, Switzerland, 2019, ch. 10, pp. 325–366.

69 B. Meyer, *Chem. Rev.*, 1976, **76**, 367–388.

70 J. J. Griebel, N. A. Nguyen, A. V. Astashkin, R. S. Glass, M. E. Mackay, K. Char and J. Pyun, *ACS Macro Lett.*, 2014, **3**, 1258–1261.

71 Y. Yoon, K. Ganapathi and S. Salahuddin, *Nano Lett.*, 2011, **11**, 3768–3773.



72 Q. H. Wang, K. Kalantar-Zadeh, A. Kis, J. N. Coleman and M. S. Strano, *Nat. Nanotechnol.*, 2012, **7**, 699–712.

73 H. Wang, L. Yu, Y.-H. Lee, Y. Shi, A. Hsu, M. L. Chin, L.-J. Li, M. Dubey, J. Kong and T. Palacios, *Nano Lett.*, 2012, **12**, 4674–4680.

74 H. Qiu, L. Pan, Z. Yao, J. Li, Y. Shi and X. Wang, *Appl. Phys. Lett.*, 2012, **100**, 123104.

75 S. Tongay, J. Suh, C. Ataca, W. Fan, A. Luce, J. S. Kang, J. Liu, C. Ko, R. Raghunathanan, J. Zhou, F. Ogletree, J. Li, J. C. Grossman and J. Wu, *Sci. Rep.*, 2013, **3**, 2657.

76 D. J. Late, B. Liu, H. S. S. R. Matte, V. P. Dravid and C. N. R. Rao, *ACS Nano*, 2012, **6**, 5635–5641.

77 N. Kaushik, D. M. A. Mackenzie, K. Thakar, N. Goyal, B. Mukherjee, P. Boggild, D. H. Petersen and S. Lodha, *npj 2D Mater. Appl.*, 2017, **1**, 34.

78 J. Kim, B. Seo, S. H. Lee, S. W. Jeong and Y. Roh, *J. Nanosci. Nanotechnol.*, 2017, **17**, 7327–7330.

79 M. Gu, T. Kim, D. Jeon, D. Lee, J. Park and T. Kim, *ACS Appl. Electron. Mater.*, 2024, **6**, 8525–8531.

80 Z. Hu, Z. Wu, C. Han, J. He, Z. Ni and W. Chen, *Chem. Soc. Rev.*, 2018, **47**, 3100–3128.

81 W. Zhu, T. Low, Y.-H. Lee, H. Wang, D. B. Farmer, J. Kong, F. Xia and P. Avouris, *Nat. Commun.*, 2014, **5**, 3087.

82 H. Jung, M. Kim, Y. Lee, G. B. Sim, H. Gu, S. Hong, S. Lee, J. Lee, D. Lee, T. Zou, K. Kang, C. W. Myung, Y.-Y. Noh and J. Kwon, *ACS Nano*, 2025, **19**, 6069–6078.

83 S. M. Sze and K. K. Ng, in *Physics of Semiconductor Devices*, ed. S. M. Sze and K. K. Ng, John Wiley & Sons, Inc., Hoboken, NJ, USA, 3rd edn, 2006, ch. 6, pp. 293–373.

